

Feature Perturbation Augmentation for Reliable Evaluation of Importance Estimators in Neural Networks*

Lennart Brocki, Neo Christopher Chung

^aInstitute of Informatics, University of Warsaw, Banacha 2, Warsaw, 02-097, , Poland

Abstract

Post-hoc explanation methods attempt to make the inner workings of deep neural networks more comprehensible and trustworthy, which otherwise act as black box models. However, since a ground truth is in general lacking, local post-hoc explanation methods, which assign importance scores to input features, are challenging to evaluate. One of the most popular evaluation frameworks is to perturb features deemed important by an explanation and to measure the change in prediction accuracy. Intuitively, a large decrease in prediction accuracy would indicate that the explanation has correctly quantified the importance of features with respect to the prediction outcome (e.g., logits). However, the change in the prediction outcome may stem from perturbation artifacts, since perturbed samples in the test dataset are out of distribution (OOD) compared to the training dataset and can therefore potentially disturb the model in an unexpected manner. To overcome this challenge, we propose feature perturbation augmentation (FPA) which creates and adds perturbed images during the model training. Our computational experiments suggest that FPA makes the considered models more robust against perturbations. Overall, FPA is an intuitive and straightforward data augmentation technique that renders the evaluation of post-hoc explanations more trustworthy

Reproducible codes and pre-trained models with FPA are available on Github: <https://github.com/lenbrocki/Feature-Perturbation-Augmentation>.

*Early version at the ICLR 2023 Workshop on Trustworthy ML; Full paper published in *Pattern Recognition Letters* doi:10.1016/j.patrec.2023.10.012

Keywords: deep neural network, interpretability, explainability, importance estimator, saliency map, data augmentation

1. Introduction

Deep learning exhibits state-of-the-art performance in a wide range of computer vision tasks. However, the reasons underlying classifications and predictions made by deep neural networks (DNN) are difficult to extract due to their nested non-linear structure and a large number of parameters [1]. Post-hoc explanations, which estimate the importance of input features with respect to the model’s output [2, 3, 4], are often used to make deep learning models more interpretable. However, evaluating the fidelity of post-hoc importance estimators is highly convoluted due to a lack of ground truth and the issue of unintentionally triggering perturbation artifacts. In this study, we introduce *feature perturbation augmentation (FPA)* which aims to avoid the pitfalls of a perturbation-based evaluation of interpretability methods.

A promising approach for comparing importance estimators despite the aforementioned lack of ground truth is the perturbation of input features [5, 6, 7]. Conceptually, if the model’s accuracy rapidly decreases by masking pixels deemed most important by some estimator, then it can be concluded that the considered estimator describes the model more accurately than others which result in a slower decrease. However, such an evaluation by perturbation may be problematic due to the risk of unwittingly triggering artifacts of the deep learning model [8, 9]. In other words, even when truly unimportant pixels are masked, the accuracy might decrease considerably nonetheless, casting doubt on the reliability of the perturbation-based evaluation approach. This issue is closely related to adversarial examples [10], which are small, but worst-case, perturbations of input images that cause the model to output a wrong prediction with high confidence.

Our proposed approach mitigates the influence of perturbation artifacts by training the model with data augmentation that reflects the perturbation used in the evaluation frameworks. We apply the proposed methods on three datasets (CIFAR-10 [11], Food101 [12], the ImageNet [13]), using four different post-hoc explanation methods. Subsequently, we measure the model output while perturbing an increasing fraction of input features sorted either in most important first (MIF) or least important first (LIF) order. MIF and

LIF perturbation curves demonstrate that when using FPA during training, the resulting model exhibits increased robustness against perturbation artifacts, and the evaluation of importance estimators becomes more reliable.

In Sec. 2, we briefly review existing evaluation methods for importance estimators and explain how our approach relates to them. Sec. 3 describes in detail the proposed feature perturbation augmentation, the model architectures and datasets, and the importance estimators under consideration. In Sec. 4, we present the results of our experiments, which demonstrate how FPA makes our evaluations more reliable. We also discuss interesting implications of our results concerning the sign fluctuations that importance estimators often exhibit. Finally, the discussion and conclusion follow in Sec. 5 and Sec. 6, respectively.

2. Related work

The explainability of deep learning is an active and diverse area of research (see [14] for a recent review). In this work, we focus on post-hoc explanations, which aim to render the inner workings of a previously trained model more transparent and understandable. In contrast, inherently interpretable models are designed from the ground up to provide explanations for their decision-making processes [15]. In order to characterize and improve post-hoc interpretability methods, it is imperative to consider what are the desired properties (desiderata) and how to evaluate them. Some of the proposed desiderata include, but are not limited to, faithfulness, localization [16, 17, 18], sparsity[18], and fulfillment of certain axiomatic properties [4].

Faithfulness or *fidelity* describes how accurately explanation methods estimate the contribution of input features to the model’s predictions. Our study falls into this category, and is related to pixel-flipping [19], region-perturbation [5], and Remove and Retrain (ROAR) [8]. All these methods perturb input pixels and measure the resulting change in model performance. Our proposed approach is similar to Remove and Retrain (ROAR)[8] in so far as it also requires retraining the model but it differs in important aspects. In ROAR, for example, the model is re-trained repeatedly with an increasing fraction of the most important input pixels masked, where the ranking of pixels is established by applying an importance estimator on the original model (trained without any perturbation). In contrast, the proposed *Feature Perturbation Augmentation* trains the model only once without using the knowledge of the importance estimator and uses the same model for

subsequent evaluation.

Other methods to evaluate faithfulness include *faithfulness correlation* [20] and *sensitivity-n* [21], which measure the correlation between the sum of importance scores of masked pixels and the delta in model output. [22] proposes to crop images to a region deemed important and feed the resized crop back to the model. It is asserted that a good explanation minimizes the area of the crop while maintaining the model’s performance. The method of *Performance Information Curves* [23] applies a bokeh filter to input images and removes the filter patch-wise starting from the most important patches. The resulting softmax activations are then plotted over the “entropy” of the perturbed images. There exist several other methods, which are often variations of one of the methods described above: ROAD [24], IROF [25], Infidelity [26] and Sufficiency [27].

Data augmentation can make machine learning models more robust and generalizable. From noise injection to utilizing DNNs for creating synthetic data, there are many data augmentation techniques (see a review [28]). In deep learning, one may apply geometric and color manipulations, make use of noise and filters, and modify feature space. The closest approach to the proposed FPA method is “random erasing” [29]. Random erasing augments the data by randomly selecting a rectangle region in an image and replacing its pixels with non-informative values such as white, black, or random RGB values. When training DNNs with random erasing, the resulting model’s performance shows increased robustness against occlusion with random rectangles [29]. FPA may be seen as a generalization and mixture of noise injection and random erasing where rectangles of varying sizes are probabilistically used to perturb the input data. Of course, the aim of FPA is very different from other data augmentations techniques, since we focus on improving interpretability rather than classifying performance [30].

3. Methods and Materials

Feature Perturbation Augmentation

The perturbation-based evaluation of importance estimators has been criticized [8] since the perturbation of input pixels leads to a shift in the data distribution, violating the key assumption that training and test data stem from the same distribution. It is then unclear whether the observed degradation of model performance is due to this out-of-distribution (OOD) problem or the removal of truly informative features. See [9] for concrete examples of



Figure 1: Examples of feature perturbation augmentation (FPA) applied on *Left*: CIFAR-10 and *Right*: ImageNet.

how pixel perturbations can act as adversarial attacks. In fact, [14] argues that certain importance estimators perform very well in perturbation-based evaluations because they strongly trigger perturbation artifacts and not because they faithfully describe the model.

We propose to overcome this problem by augmenting the data during training using the same kind of data perturbations that will be used for the subsequent evaluation of post-hoc importance estimators. If features are to be masked by setting them to zero, as in our experiments, the training data shall be augmented with samples that have randomly selected pixels set to zero. In this way, FPA mitigates the risk of the OOD problem and one can be more confident that a perturbation-based evaluation of importance estimators actually quantifies the removal of information that is relevant for the model’s predictions.

In FPA, mini-batches in training are selected for perturbation with a probability p . Within a selected image, we iterate through input features; p^1 refers to the probability of masking a single pixel and p^2 refers to the probability of creating a non-informative square. For concreteness, p^2 is selected from a range $(0, 1)$ for all mini-batches. Then, the perturbation is defined as follows. First, for each mini-batch, we draw p^1 from $\text{Uniform}(0, p_{\max}^1)$ distribution and set input pixels to 0 with a probability of p^1 . Second, with a probability of p^2 for each selected pixel, we create a non-informative square of 0’s, with a randomly chosen side length in the interval $[1, s_{\max}]$. This specific definition of perturbations is of heuristic nature and we found it to work well in our experiments. It is by no means unique or optimal and many other design choices are possible. See details in the Algorithm 1.

Besides masking pixels with zeros, many different schemes of masking are possible, such as setting pixels to random, minimum, or maximum values or applying blurring, bokeh, or other filters. Similar to an ambiguous prob-

Algorithm 1 Feature Perturbation Augmentation in a Selected Mini-batch

Require: K samples $\mathbf{X}_{w,h,c}^k$ for $k = 0, \dots, K$, where \mathbf{X}^k is of dimension $W \times H \times C$.

Require: $s_{\max} < \min(W, H)$, $p_{\max}^1 \in (0, 1)$, $p^2 \in (0, 1)$

Set $p^1 \sim \text{Uniform}(0, p_{\max}^1)$

for $k \leftarrow 0$ to K

for $w \leftarrow 0$ to W

for $h \leftarrow 0$ to H

 With p^1 , $\mathbf{X}_{w,h}^k \leftarrow 0$ (i.e., a non-informative value).

 Set $s \leftarrow \{1, 2, \dots, s_{\max}\}$

 With p^2 , $\mathbf{X}_{w:(w+s),h:(h+s)}^k \leftarrow 0$ (i.e., a $s \times s$ square of non-informative values).

lem of choosing a non-informative baseline for integrated gradients [4, 31], perturbation should reflect the application domain. Beyond the specific implementation (Algorithm 1), our proposal is generally applicable. To make perturbation-based interpretability evaluate more reliable, one should include similarly perturbed samples during training.

Datasets and Importance Estimators

We demonstrate our approach using two popular deep learning architectures and three datasets, namely the ResNet-50 [32] architecture trained on ImageNet [13] and Food101 [12], and ResNet-18 trained on CIFAR-10 [11], see Appendix A for details concerning the datasets and training procedure. We compare the following four importance estimators: vanilla gradient (VG) [2], integrated gradients (IG) [4], SmoothGrad (SG) [3] and squared SmoothGrad (SQ-SG) [8].

These methods output three-dimensional maps of importance scores (height, width, and color channels). To obtain two-dimensional maps for the pixel-wise perturbation, we explore two variants: *unsigned* and *signed*. First, for the unsigned estimators, we sum the absolute values of color channels, which are denoted by the subscript _{abs}. In this case, very small values ($\gtrsim 0$) have minimal influence on that prediction. Second, for the signed estimators, we multiply the raw importance scores element-wise with the input image [33], (indicated by a prime) and sum over the resulting color channels (indicated by a subscript _{sum}). For example, VG'_{sum} . Negative importance scores from the signed estimators may imply *counter-evidence* for the predicted class. IG

includes a multiplication with the input by definition and will therefore not appear primed.

We note that VG' is equivalent to ϵ -LRP [19] when non-linearities are ReLUs [21], as in the ResNet architectures. Furthermore, multiplication with the input should be used with caution, since important pixels can be assigned, erroneously, a zero or low score when they are multiplied with a zero or low pixel value [34, 31]. See Appendix B for more details about the importance estimators.

Fidelity of Importance Estimators

Perturbation-based evaluation methods are both intuitive and popular [5, 6, 7]. For our evaluation of fidelity, we create *perturbation curves* of changes in logits, i.e. pre-softmax activations in the prediction vector, with respect to an increasing amount of perturbation (e.g., Fig. 2). When needed for comparison, logits are normalized against the original model prediction without any masked pixel, e.g. in Fig. 3. A given importance estimator computes a set of importance scores for input pixels, which indicate how much each pixel contributed to the final prediction. Then, input pixels are perturbed in order of either the most important first (MIF) or the least important first (LIF) [35]. In the case of signed importance scores, the ranking goes from the highest positive values to the lowest negative ones (MIF), or reversely (LIF). Therefore, the lowest negative importance scores, which are ranked first in LIF, may indicate strong counter-evidence for the predicted class.

When the importance estimator deems a certain feature important, ideally the removal of this feature would strongly decrease the associated logit. A greater logit decrease would imply that a chosen feature is more important for the model’s prediction. Inversely, if a feature has a low-ranked importance score, its removal would lead to a minimal accuracy decrease (unsigned estimators) or potentially an accuracy increase for removing counter-evidence

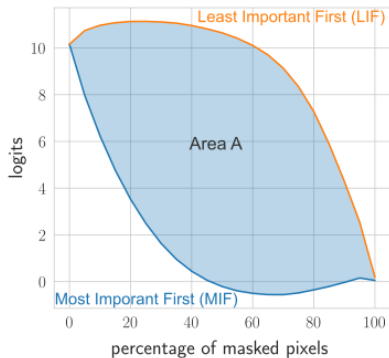


Figure 2: The fidelity metric A is defined as the area between the LIF (orange) and MIF (blue) curves. Importance estimators with larger A are considered to explain the model more accurately.

(signed estimators). To obtain the final perturbation curves, we average normalized logits over all 10,000 samples in the test set for CIFAR-10. For ImageNet and Food101, we average over a randomly selected subset of 5,000 samples from the test set.

In order to combine these two aspects, we use the area A between the MIF and LIF curves (Fig. 2) as a metric to measure the relative fidelity of importance estimators. A small area under the MIF curve indicates that the estimator is good at detecting features that are important evidence for a given class. A large area under the LIF curve, on the other hand, means that the estimator can reliably find unimportant features; negative importance scores (e.g., gradients) would imply counter-evidence for the prediction. With A as fidelity metric, we, therefore, consider importance estimators with large A to be overall superior to ones with lower A .

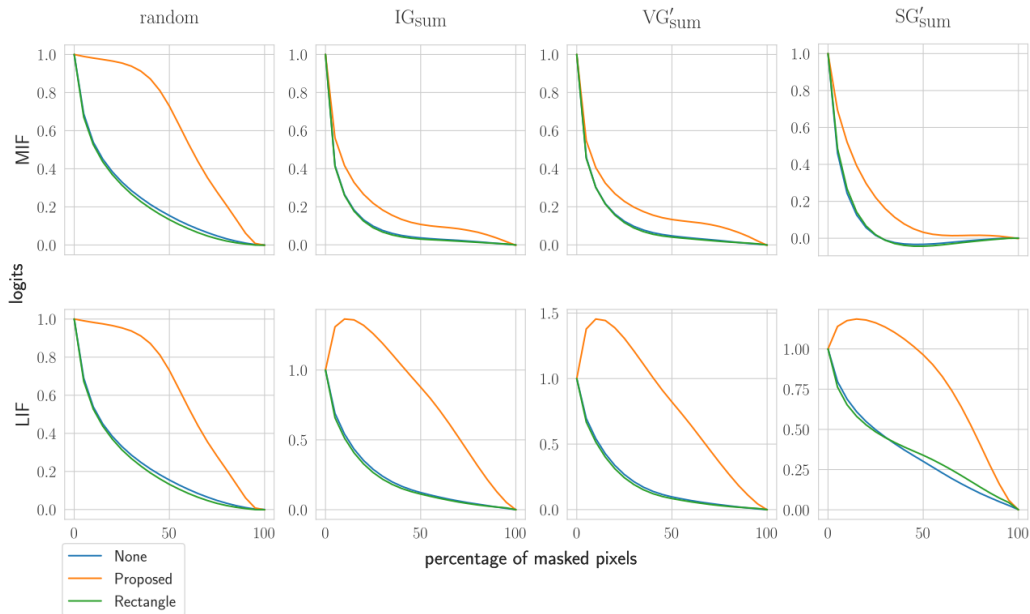


Figure 3: Perturbation curves for the ResNet-50 trained on Food101 data with importance scores obtained using *signed importance estimators*, i.e. both positive and negative importance scores available. “Rectangle” refers to the data augmentation proposed in [29]. “Random” (far left) means that importance scores are randomly assigned and the initial, unperturbed, logits have been normalized to one.

4. Results

4.1. Accuracy of models

We applied the proposed FPA on three datasets; the ImageNet [13], Food101 [12], and CIFAR-10 [11]. The ResNet-50 [32] architecture is used for ImageNet and Food101 and ResNet-18 for CIFAR-10. Desirable parameters for FPA significantly improve the model’s robustness while maintaining its accuracy. In order to find a good set of parameters we performed a partial grid search, keeping p^2 and s_{\max} fixed and varying p in the range $[0.2, 0.5]$ and p_{\max}^1 in $[0.1, 0.4]$ using 0.1 and 0.5 steps for Food101 and CIFAR-10, respectively. Due to restrictions in computing resources, we did not include p^2 and s_{\max} in the grid search. FPA parameters for the ImageNet were set to the same parameters selected for Food101. For the augmentation of CIFAR-10, we chose $p_{\max}^1 = 0.25$, $p^2 = 0.1$, $s_{\max} = 3$ and for ImageNet and Food101 $p_{\max}^1 = 0.3$, $p^2 = 0.01$, $s_{\max} = 10$. We set $p = 0.5$ for all three datasets. The chosen parameter values present a good trade-off between the increased robustness and performance of the model.

Evaluated on the same images that are used to obtain the perturbation curves, the models trained on CIFAR-10 have an accuracy of 93.0%, 92.7% and 93.1% for no augmentation, proposed FPA and “random erasing” [29] (denoted as “Rectangle” in our figures), respectively. In the same order, the models trained on ImageNet have an accuracy of 76.2%, 74.7% and 75.9% and on Food101 83.5%, 81.5% and 83.5%.

4.2. Perturbation curves

Once the model is trained with or without data augmentation, vanilla gradient (VG), integrated gradient (IG), Smoothgrad (SG), and squared SmoothGrad (SQ-SG) are applied to obtain matrices of importance scores. We also calculate perturbation curves as described in Sec. 3. In Fig. 3, the MIF perturbation curves (top row) fall off slower when the model was trained with the proposed FPA, compared to those with no augmentation or Rectangle augmentation [29]. For LIF perturbation curves (bottom row, Fig. 3) the logits initially increase before decreasing if FPA is used. In contrast, without any augmentation or with “Rectangle” augmentation, the logits immediately and rapidly decrease. The random baseline (where importance scores are randomly assigned to pixels) does not exhibit the early increase of logits.

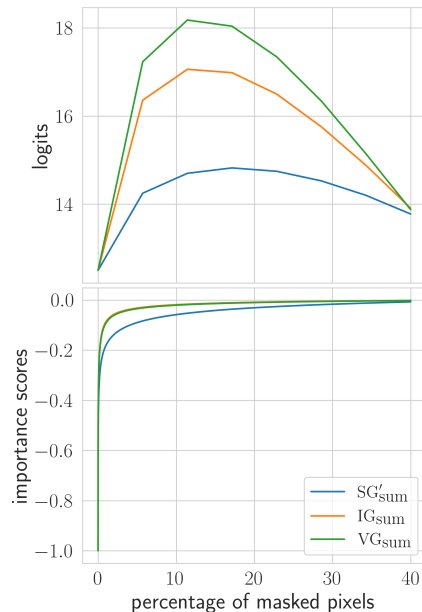


Figure 4: Comparison of the model output and importance scores when FPA is used. Masking pixels with negative importance scores coincides with increasing logit values. *Top*: LIF perturbation curves of logits for Food101. *Bottom*: Importance scores of pixels that are masked in the LIF order.

These operating characteristics are expected when the influence of artifacts is removed, or at least strongly reduced, by our proposed augmentation. Generally, some of the logit decrease is expected to be due to perturbation artifacts, thus removing perturbation artifacts would delay the logit decrease. In the LIF curves in Fig. 3, pixels with large negative importance scores are masked first which removes *counter-evidence*. This is highlighted in Fig. 4, which demonstrates that masking pixels with a negative importance score coincides with an increase in the logit values (see Fig. Appendix C.3 for equivalent graphs for CIFAR-10 and ImageNet). In contrast, without FPA, this effect is suppressed and we hypothesize that this is due to perturbation artifacts disturbing the model. This would lead to a net decrease of the logits, despite pixels with negative scores, i.e. counter-evidence, being masked. This behavior is consistent across the three considered datasets and architectures (see Figs. Appendix C.1 and Appendix C.2).

4.3. Comparing fidelity of importance estimators

We compare the fidelity A of importance estimators (Tabs. 1, Appendix D.1 and Appendix D.2) considering two different settings. In the first setting, we take into account the magnitude of importance scores and disregard whether their signs correctly indicate evidence or counter-evidence for the prediction. Non-negative importance scores are obtained from the *unsigned estimators*: IG_{abs} , VG_{abs} , VG'_{abs} , SG_{abs} , SG'_{abs} and $SQ\text{-}SG_{\text{sum}}$. Among those that rank pixels purely by the magnitude of importance scores, we find that across all three considered datasets, and regardless of the augmentation, $SQ\text{-}SG_{\text{sum}}$ consistently performs best and VG_{abs} worst.

Table 1: The fidelity of importance estimators A (the area between LIF and MIF perturbation curves), measured on the ResNet-50 trained on Food101 with 95% confidence intervals.

Aug.	Random	IG_{sum}	IG_{abs}	VG_{abs}	VG'_{sum}
None	0.0 ± 0.8	11.6 ± 0.7	22.6 ± 0.8	15.5 ± 0.8	8.7 ± 0.6
Proposed	0.0 ± 0.6	67.7 ± 1.0	29.4 ± 0.6	24.8 ± 0.7	66.0 ± 1.0
Aug.	VG'_{abs}	SG_{abs}	SG'_{sum}	SG'_{abs}	$SQ\text{-}SG_{\text{sum}}$
None	15.5 ± 0.8	22.2 ± 0.8	30.3 ± 0.8	23.7 ± 0.7	31.2 ± 0.8
Proposed	24.8 ± 0.7	28.9 ± 0.7	69.4 ± 0.9	27.0 ± 0.6	31.3 ± 0.7

For the second setting, we consider signed importance scores from the *signed estimators*; namely, IG_{sum} , VG'_{sum} and SG'_{sum} , which multiply the gradients and input element-wise¹. With FPA, the signed estimators consistently outperform the unsigned ones across all three datasets, with IG_{sum} and SG'_{sum} in the leading positions. Intuitively, this makes sense since the signed estimators contain more information than the unsigned ones, allowing them to describe the models' predictions more accurately.

4.4. Fluctuations in the sign of importance scores

¹Notice that the gradients by themselves, without multiplying with the input, can not correctly infer the sign of importance scores. This becomes clear when one considers a linear model $f(x) = \omega x$, the gradient $\frac{\partial f}{\partial x} = \omega$ does not contain information on the sign of f if x can be negative. Multiplying with the input yields $x \frac{\partial f}{\partial x}$ and thus VG' gives the correct sign in the linear case. IG has a multiplication with the input built into its definition.

The high-frequency fluctuations in the sign of importance scores have previously been attributed to the inability of importance estimators to predict the sign accurately [21, 14]. However, our results demonstrate that the observed fluctuations describe the model characteristics rather accurately if perturbation artifacts are suppressed by FPA. For illustrative purposes, we focus on a randomly chosen sample in Fig. 5. The trained ResNet-50 model is generally focusing on the object of interest (correctly predicted as “beef tartare”), but we also observe that within that object, the sign of importance scores fluctuates. The distribution of negative (Fig. 5(e)) and positive (Fig. 5(f)) importance scores are highly concentrated ($\sim 2\%$ of all pixels each).

We further created a truncated heatmap (Fig. 5(c)) where only the highest and lowest importance scores are plotted (thresholding at the 98th percentile), highlighting only those pixels whose removal causes the initial increase and decrease in logits in Fig. 5(d). The vast majority of those pixels are within the region of interest (ROI). Finally, the right-side plots (Fig. 5(d-f)) show that the initial increase (or decrease) of logits in the LIF (or MIF) curve coincides with masking large negative (or positive) values. Taken together, these observations imply that the sign fluctuations may actually be meaningful.

5. Discussion

As this work has been focused on the interpretability and trustworthiness of deep learning models, there still is room for performance improvement. Training the models with FPA leads to a slight decrease in performance compared to training them without augmentation. This might be due to “augment ambiguity” [36], which occurs when the annotated class is not recognizable anymore as a result of an augmentation. On the other hand,

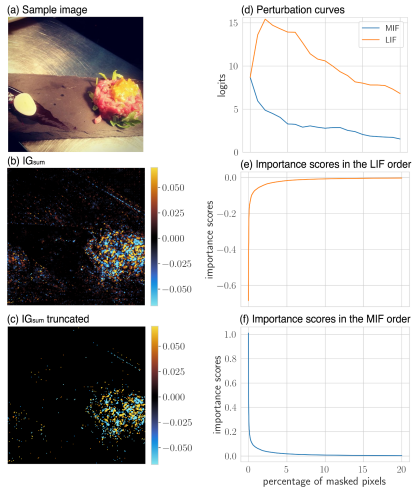


Figure 5: Explainability of the sign of importance scores and perturbation curves, using a sample image from Food101 (correctly classified as “beef tartare”). In (c), pixels with IG_{sum} scores lower than the 98th percentile are set to zero, and the importance scores are clipped at the 99th percentile.

random erasing, which is closely related to FPA, reported an increase in the model performance in certain settings [29]. In future work, we plan to explore variations of FPA and training schemes to mitigate the performance loss, but also point out that trading some accuracy for increased interpretability can be worthwhile.

Our results show that VG, SG, and IG outperform a random baseline across all three considered datasets. Comparing our ranking of importance estimators to those in the literature we find that, in contrast to our results, ROAR [8] reports that VG, SG, and IG perform worse than a random baseline. Several other evaluation methods, however, report that IG performs better than a random baseline as well [23, 25, 21]. We hypothesize that the counter-intuitive results of ROAR arise because, by measuring the accuracy of the retrained models (cf. Sec. 2), one gauges how much information has been removed and was not available for retraining the model. In general, this is different from gauging how much information has been removed *that the original model relies on*. Our proposed method avoids this pitfall by training the model only once with FPA and then using the same model for all following evaluations. Similar concerns with ROAR have been raised in [37].

Furthermore, the performed experiments bring out an interesting insight into the frequently observed fluctuation of the sign of importance scores obtained from gradient-based or LRP methods. Often, these fluctuations have been attributed to a failure of post-hoc explanations to correctly predict the sign and are considered an issue that requires fixing [23, 21, 14]. Our results imply that these fluctuations may not be a bug but a feature. To arrive at its predictions, the model often focuses on the ROI, but within, it may find rapidly alternating evidence and counter-evidence on the pixel-level. Deep neural networks and humans appear to arrive at their predictions in very different ways and we would therefore caution against forcing post-hoc explanations to align with human expectations.

Concerning possible extensions of our work, notice that since FPA randomly selects pixels to construct augmented training samples it can be expected to only increase a model’s robustness against such random perturbations. To increase the robustness against adversarial perturbations our work could be extended by additionally performing adversarial training [10, 38], which would allow to rule out perturbation artifacts during evaluation with even higher confidence.

6. Conclusions

We demonstrate that the perturbation-based evaluation of importance estimators for deep neural networks (DNNs) can be made more reliable by our proposed feature perturbation augmentation (FPA). Our experiments using the Most Important First (MIF) and Least Important First (LIF) perturbation curves demonstrate that our FPA training makes the DNNs more robust against perturbations and this effectively mitigates the issue of confounding artifacts introduced by masking input pixels during interpretability evaluation. To the best of our knowledge, FPA is the first data augmentation technique specifically developed to improve the evaluation of interpretability methods in DNNs.

Acknowledgements

This work was funded by the ERA-Net CHIST-ERA grant [CHIST-ERA-19-XAI-007] long term challenges in ICT project INFORM (ID: 93603), by the National Science Centre (NCN) of Poland [2020/02/Y/ST6/00071]. This research was carried out with the support of the Interdisciplinary Centre for Mathematical and Computational Modelling University of Warsaw (ICM UW) under computational allocation no GDM-3540; the NVIDIA Corporation’s GPU grant; and the Google Cloud Research Innovators program.

References

- [1] W. Samek, G. Montavon, A. Vedaldi, L. K. Hansen, K.-R. Müller, *Explainable AI: interpreting, explaining and visualizing deep learning*, Vol. 11700, Springer Nature, 2019.
- [2] K. Simonyan, A. Vedaldi, A. Zisserman, *Deep inside convolutional networks: Visualising image classification models and saliency maps*, in: *In Workshop at International Conference on Learning Representations*, Citeseer, 2014.
- [3] D. Smilkov, N. Thorat, B. Kim, F. Viégas, M. Wattenberg, *Smoothgrad: removing noise by adding noise*, arXiv preprint arXiv:1706.03825 (2017).
- [4] M. Sundararajan, A. Taly, Q. Yan, *Axiomatic attribution for deep networks*, in: *International conference on machine learning*, PMLR, 2017, pp. 3319–3328.

- [5] W. Samek, A. Binder, G. Montavon, S. Lapuschkin, K.-R. Müller, Evaluating the visualization of what a deep neural network has learned, *IEEE transactions on neural networks and learning systems* 28 (11) (2016) 2660–2673.
- [6] V. Petsiuk, A. Das, K. Saenko, Rise: Randomized input sampling for explanation of black-box models, *arXiv preprint arXiv:1806.07421* (2018).
- [7] P.-J. Kindermans, K. T. Schütt, M. Alber, K.-R. Müller, D. Erhan, B. Kim, S. Dähne, Learning how to explain neural networks: Patternnet and patternattribution, *arXiv preprint arXiv:1705.05598* (2017).
- [8] S. Hooker, D. Erhan, P.-J. Kindermans, B. Kim, A benchmark for interpretability methods in deep neural networks, *Advances in neural information processing systems* 32 (2019).
- [9] R. C. Fong, A. Vedaldi, Interpretable explanations of black boxes by meaningful perturbation, in: *Proceedings of the IEEE international conference on computer vision*, 2017, pp. 3429–3437.
- [10] I. J. Goodfellow, J. Shlens, C. Szegedy, Explaining and harnessing adversarial examples, *arXiv preprint arXiv:1412.6572* (2014).
- [11] A. Krizhevsky, Learning multiple layers of features from tiny images, *University of Toronto Technical Report* (2009).
- [12] L. Bossard, M. Guillaumin, L. V. Gool, Food-101—mining discriminative components with random forests, in: *European conference on computer vision*, Springer, 2014, pp. 446–461.
- [13] J. Deng, W. Dong, R. Socher, L.-J. Li, K. Li, L. Fei-Fei, Imagenet: A large-scale hierarchical image database, in: *2009 IEEE conference on computer vision and pattern recognition*, Ieee, 2009, pp. 248–255.
- [14] W. Samek, G. Montavon, S. Lapuschkin, C. J. Anders, K.-R. Müller, Explaining deep neural networks and beyond: A review of methods and applications, *Proceedings of the IEEE* 109 (3) (2021) 247–278.
- [15] C. Rudin, C. Chen, Z. Chen, H. Huang, L. Semenova, C. Zhong, Interpretable machine learning: Fundamental principles and 10 grand challenges, *Statistics Surveys* 16 (2022) 1–85.

- [16] A. Saporta, X. Gui, A. Agrawal, A. Pareek, S. Q. Truong, C. D. Nguyen, V.-D. Ngo, J. Seekins, F. G. Blankenberg, A. Y. Ng, et al., Benchmarking saliency methods for chest x-ray interpretation, *Nature Machine Intelligence* (2022) 1–12.
- [17] L. Brocki, W. Marchadour, J. Maison, B. Badic, P. Papadimitroulas, M. Hatt, F. Vermet, N. C. Chung, Evaluation of importance estimators in deep learning classifiers for computed tomography, in: *International Workshop on Explainable, Transparent Autonomous Agents and Multi-Agent Systems*, Springer, 2022, pp. 3–18.
- [18] B. Zhou, A. Khosla, A. Lapedriza, A. Oliva, A. Torralba, Learning deep features for discriminative localization, in: *Proceedings of the IEEE conference on computer vision and pattern recognition*, 2016, pp. 2921–2929.
- [19] S. Bach, A. Binder, G. Montavon, F. Klauschen, K.-R. Müller, W. Samek, On pixel-wise explanations for non-linear classifier decisions by layer-wise relevance propagation, *PloS one* 10 (7) (2015) e0130140.
- [20] U. Bhatt, A. Weller, J. M. Moura, Evaluating and aggregating feature-based model explanations, *arXiv preprint arXiv:2005.00631* (2020).
- [21] M. Ancona, E. Ceolini, C. Öztireli, M. Gross, Towards better understanding of gradient-based attribution methods for deep neural networks, *arXiv preprint arXiv:1711.06104* (2017).
- [22] P. Dabkowski, Y. Gal, Real time image saliency for black box classifiers, *Advances in neural information processing systems* 30 (2017).
- [23] A. Kapishnikov, T. Bolukbasi, F. Viégas, M. Terry, Xrai: Better attributions through regions, in: *Proceedings of the IEEE/CVF International Conference on Computer Vision*, 2019, pp. 4948–4957.
- [24] Y. Rong, T. Leemann, V. Borisov, G. Kasneci, E. Kasneci, A consistent and efficient evaluation strategy for attribution methods, in: *International Conference on Machine Learning*, PMLR, 2022, pp. 18770–18795.
- [25] L. Rieger, L. K. Hansen, Irof: a low resource evaluation metric for explanation methods, *arXiv preprint arXiv:2003.08747* (2020).

- [26] C.-K. Yeh, C.-Y. Hsieh, A. Suggala, D. I. Inouye, P. K. Ravikumar, On the (in) fidelity and sensitivity of explanations, *Advances in Neural Information Processing Systems* 32 (2019).
- [27] S. Dasgupta, N. Frost, M. Moshkovitz, Framework for evaluating faithfulness of local explanations, *arXiv preprint arXiv:2202.00734* (2022).
- [28] C. Shorten, T. M. Khoshgoftaar, A survey on image data augmentation for deep learning, *Journal of big data* 6 (1) (2019) 1–48.
- [29] Z. Zhong, L. Zheng, G. Kang, S. Li, Y. Yang, Random erasing data augmentation, in: *Proceedings of the AAAI conference on artificial intelligence*, Vol. 34, 2020, pp. 13001–13008.
- [30] G. K. Dziugaite, S. Ben-David, D. M. Roy, Enforcing interpretability and its statistical impacts: Trade-offs between accuracy and interpretability, *arXiv preprint arXiv:2010.13764* (2020).
- [31] P. Sturmfels, S. Lundberg, S.-I. Lee, Visualizing the impact of feature attribution baselines, *Distill* 5 (1) (2020) e22.
- [32] K. He, X. Zhang, S. Ren, J. Sun, Deep residual learning for image recognition, in: *Proceedings of the IEEE conference on computer vision and pattern recognition*, 2016, pp. 770–778.
- [33] A. Shrikumar, P. Greenside, A. Kundaje, Learning important features through propagating activation differences, in: *International conference on machine learning*, PMLR, 2017, pp. 3145–3153.
- [34] L. Brocki, N. C. Chung, Input bias in rectified gradients and modified saliency maps, in: *2021 IEEE International Conference on Big Data and Smart Computing (BigComp)*, IEEE, 2021, pp. 148–151.
- [35] L. Brocki, N. C. Chung, Evaluation of interpretability methods and perturbation artifacts in deep neural networks (2022).
- [36] L. Wei, A. Xiao, L. Xie, X. Zhang, X. Chen, Q. Tian, Circumventing outliers of autoaugment with knowledge distillation, in: *Computer Vision–ECCV 2020: 16th European Conference, Glasgow, UK, August 23–28, 2020, Proceedings, Part III*, Springer, 2020, pp. 608–625.

- [37] A.-P. Nguyen, M. R. Martínez, On quantitative aspects of model interpretability, arXiv preprint arXiv:2007.07584 (2020).
- [38] A. Madry, A. Makelov, L. Schmidt, D. Tsipras, A. Vladu, Towards deep learning models resistant to adversarial attacks, in: International Conference on Learning Representations.

Appendix A. Datasets and Training Procedure

We demonstrate our approach using two popular deep learning architectures and three datasets, namely the ResNet-50 [32] architecture trained on ImageNet [13] and Food101 [12], and ResNet-18 trained on CIFAR-10 [11]. We adapted the ResNet-18 architecture to be suitable for the smaller input dimensions of CIFAR-10 by setting the kernel size of the first convolutional layer to (3, 3) and stride and padding to (1, 1). The ResNet-50 model was trained on ImageNet for 90 epochs using the SGD optimizer with momentum 0.9, weight decay 10^{-4} and initial learning rate 0.1, which we reduced by a factor of 10 on epochs 30 and 60. On Food101, Resnet-50 was trained for 68 epochs with momentum set to 0.9, weight decay 5×10^{-4} and an initial learning rate of 0.1, where a cosine annealing schedule was used to continuously reduce the learning rate to zero. The ResNet-18 model was trained for 40 epochs using the SGD optimizer with momentum 0.9, weight decay 5×10^{-4} , and initial learning rate 0.01, which we reduced by a factor of 10 on epoch 30. For CIFAR-10 and ImageNet, we scaled input images to the range $[-1, 1]$ and for Food101 we performed a z-score normalization with mean and standard deviation from the training set. In all three cases, we performed a horizontal flip with a probability of 0.5 to augment the data.

Appendix B. Importance Estimators

After the aforementioned models are trained on ImageNet [13], Food101 [12], and CIFAR-10 [11] with and without data augmentation, we applied post-hoc interpretability methods that assign importance scores to input features. In particular, we compare the following four importance estimators

- **Vanilla gradient (VG)** [2]: Gradients of the class score S_c with respect to input pixels x_i

$$\mathbf{e} = \frac{\partial S_c}{\partial x}$$

The class score S_c is the activation of the neuron in the prediction vector that corresponds to the predicted class c by the original model. Gradients are calculated with respect to logits, i.e., pre-softmax activations.

- **Integrated gradient (IG)** [4]: Average over gradients obtained from inputs interpolated between a reference point x^0 and input x

$$\mathbf{e} = (x - x^0) \times \sum_{k=1}^m \frac{\partial S_c \left(x^0 + \frac{k}{m} (x - x^0) \right)}{\partial x} \times \frac{1}{m},$$

where x^0 is chosen to be a black image and $m = 200$.

- **Smoothgrad (SG)** [3]: Average over gradients obtained from inputs with injected noise

$$\mathbf{e} = \frac{1}{n} \sum_1^n \hat{\mathbf{e}} \left(x + \mathcal{N} \left(0, \sigma^2 \right) \right),$$

where $\mathcal{N} \left(0, \sigma^2 \right)$ represents Gaussian noise with standard deviation σ , $\hat{\mathbf{e}}$ is obtained using vanilla gradient and $n = 15$.

- **Squared SmoothGrad (SQ-SG)** [8]: Variant of SmoothGrad that squares $\hat{\mathbf{e}}$ before averaging

$$\mathbf{e} = \frac{1}{n} \sum_1^n \hat{\mathbf{e}} \left(x + \mathcal{N} \left(0, \sigma^2 \right) \right)^2.$$

Generally, importance scores are three-dimensional including height, width, and color channels. To reduce them to two-dimensional maps for feature perturbation, we compute the sum of the absolute values of color channels (*unsigned*) and the sum of element-wise multiplication between the raw importance scores and the input image (*signed*). See Sec. 3 for further details.

Appendix C. Supplementary Figures

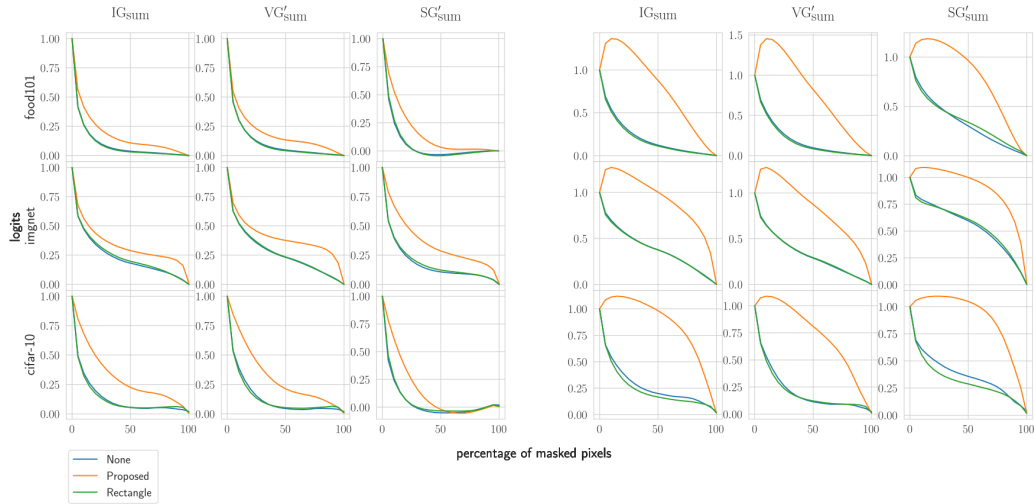


Figure Appendix C.1: Overview of perturbation curves for signed importance estimators for all three considered datasets. The raw importance scores are multiplied element-wise with the input image [33], indicated by a prime, and then followed by summing over the resulting color channels. By definition, IG includes a multiplication with the input already. The change in normalized logits is measured as a percentage of pixels that are masked according to the Most Important First (MIF; *Left*) and the Least Important First (LIF; *Right*). Note that masking pixels with negative importance scores can increase logits, as counter-evidence for the predicted class is removed from the input image.

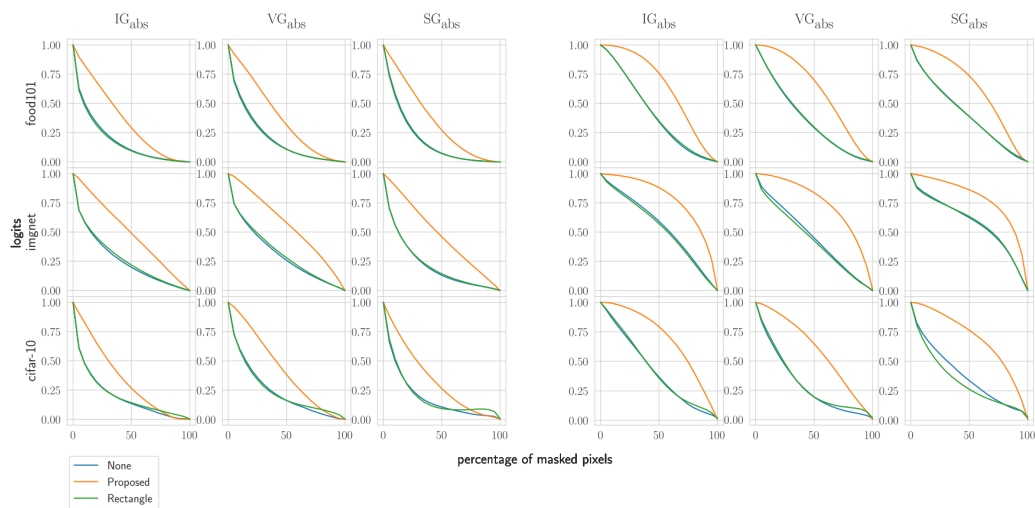


Figure Appendix C.2: Overview of perturbation curves for unsigned importance estimators for all three considered datasets. Sums of the absolute values of color channels are used. The change in normalized logits is plotted as a percentage of pixels that are masked according to the Most Important First (MIF; *Left*) and the Least Important First (LIF; *Right*). Notice that in comparison to the LIF perturbation curves from the signed estimators (Figure Appendix C.1), the initial increase for LIF perturbation does not occur for the unsigned estimators.

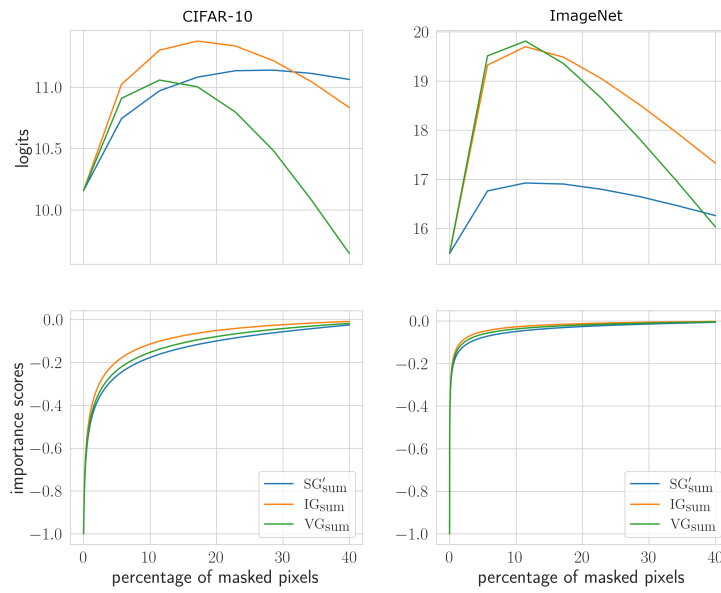


Figure Appendix C.3: *Top row:* LIF perturbation curves averaged over CIFAR-10 and ImageNet test samples. *Bottom row:* The curve has been obtained by flattening the heat map and plotting the importance scores in LIF order, with the x-axis indicating their position in the ranking. At each point on the x-axis, one can compare the importance scores of a group of pixels (y-axis labeled ‘importance scores’) and the influence of their masking on the model output (y-axis labeled ‘logits’).

Appendix D. Supplementary Tables

Table Appendix D.1: The fidelity of importance estimators A (the area between LIF and MIF perturbation curves), measured on the ResNet-50 trained on ImageNet with 95% confidence intervals. See the main text for the difference between the unsigned and signed importance estimators.

Aug.	Random	IG_{sum}	IG_{abs}	VG_{abs}	VG'_{sum}
None	0.0 ± 0.7	15.9 ± 0.7	29.2 ± 0.7	14.6 ± 0.8	6.2 ± 0.7
Proposed	0.0 ± 0.5	61.8 ± 0.8	29.2 ± 0.6	18.7 ± 0.6	45.6 ± 0.9
Aug.	VG'_{abs}	SG_{abs}	SG'_{sum}	SG'_{abs}	$SQ-SG_{\text{sum}}$
None	23.0 ± 0.8	36.4 ± 0.7	38.1 ± 0.9	40.0 ± 0.7	42.7 ± 0.6
Proposed	23.7 ± 0.6	31.0 ± 0.6	57.3 ± 0.8	33.9 ± 0.6	36.2 ± 0.6

Table Appendix D.2: The fidelity of importance estimators A (the area between LIF and MIF perturbation curves), measured on the ResNet-18 trained on CIFAR-10 with 95% confidence intervals.

Aug.	Random	IG_{sum}	IG_{abs}	VG_{abs}	VG'_{sum}
None	0.0 ± 0.7	14.0 ± 0.8	21.9 ± 0.6	5.6 ± 0.6	8.0 ± 0.7
Proposed	0.0 ± 0.5	59.6 ± 0.7	34.9 ± 0.5	16.9 ± 0.5	47.0 ± 0.7
Aug.	VG'_{abs}	SG_{abs}	SG'_{sum}	SG'_{abs}	$SQ-SG_{\text{sum}}$
None	16.1 ± 0.6	18.5 ± 0.6	34.6 ± 0.8	27.0 ± 0.6	27.9 ± 0.6
Proposed	25.8 ± 0.5	35.4 ± 0.5	80.5 ± 0.6	39.2 ± 0.5	41.1 ± 0.5